Paul Langacker

The Standard Model and Beyond

Update of Section 7.5, December 25, 2014.

www.sns.ias.edu/~pgl/SMB/
www.crcpress.com/product/isbn/9781420079067/

7.5 The Higgs

The spontaneous symmetry breaking sector has always been the most uncertain part of the standard model. The simplest possibility is that the SSB is accomplished by the VEV of an elementary Higgs doublet, as described in Section 7.2.1, or by a more complicated Higgs sector involving two or more Higgs doublets (as in the supersymmetric extension of the SM) or other representations. It is also possible that the SSB is associated with a dynamical mechanism not involving elementary scalar fields, as will be touched on at the end of this Section and in Chapter 8. The observation of a Higgs-like boson* with mass ~ 125 GeV in 2012 strongly supports the notion of an elementary Higgs doublet. However, as of this writing (in March 2014) the measurements of the Higgs couplings are not yet sufficiently precise to exclude some of the alternatives, especially limiting cases involving a boson very similar to the SM Higgs. In this section, we describe some of the theoretical constraints on the SM Higgs and some of its predicted properties for an arbitrary mass. We then discuss the searches for the Higgs, its discovery and study at the LHC, and the implications. For more detailed discussions, see (Gunion et al., 1990; Carena and Haber, 2003; Djouadi, 2008a; Aglietti et al., 2006; Gomez-Bock et al., 2007; Dittmaier and Schumacher, 2013; Altarelli, 2013; Ellis, 2013; Herrero, 2014; Logan, 2014); the Higgs Boson review by Carena, Grojean, Kado, and Sharma in (Olive et al., 2014); and the sites devoted to Higgs production, decay, and experimental constraints listed in the Web Sites section.

In the standard model there remains one physical Higgs particle H after spontaneous symmetry breaking, with a potential given by (7.40) on page 291, and gauge, self-interaction, and Yukawa couplings to fermions given in Table 7.1. The mass is $M_H = \sqrt{2\lambda}\nu$, where λ is the quartic self-coupling and $\nu \sim 246$ GeV is $\sqrt{2}\langle 0|\phi^0|0\rangle$. The couplings to a particle of mass M are always proportional to M/ν, M^2/ν, or $(M/\nu)^2$. Thus, the couplings to fermions are small except for the top quark, making the H hard to produce or detect in that way. More optimistic are gauge couplings, such as VVH where $V = W^\pm$ or Z, which are proportional to $g^2\nu \sim M_V^2/\nu$.

7.5.1 Theoretical Constraints

The Higgs mass and quartic coupling are related by

$$M_H^2 = 2\lambda\nu^2, \qquad \lambda = \frac{g^2 M_H^2}{8M_W^2} = \frac{G_F M_H^2}{\sqrt{2}}, \tag{7.196}$$

*I.e., the SM Higgs boson or something closely resembling it. In the following it will also be referred to as the "Higgs boson" or the "Higgs".

where $\nu \sim 246$ GeV and $G_F \sim 1.2 \times 10^{-5}\text{GeV}^2$ are known. The only constraint we have imposed so far on λ is (tree-level) vacuum stability, $\lambda > 0$, which would allow any M_H from 0 to ∞. However, there are a number of more stringent theoretical constraints which lead to nontrivial upper and lower bounds. In this section we consider issues related to the Higgs and gauge boson self-interactions. Other theoretical issues, involving the Higgs contribution to the vacuum energy and the higher-order corrections to the Higgs mass, are discussed in Section 8.1.

Renormalization Group Constraints

The renormalization group equations for the running gauge couplings are given for an arbitrary gauge theory in (5.33) on page 199. For the SM the β function one-loop coefficients in (5.34) are

$$\begin{aligned} b_{g_s} &= -\frac{1}{16\pi^2}\left[11 - \frac{4F}{3}\right] \xrightarrow[F=3,n_H=1]{} \frac{1}{16\pi^2}\,(-7) \\ b_g &= -\frac{1}{16\pi^2}\left[\frac{22}{3} - \frac{4F}{3} - \frac{n_H}{6}\right] \xrightarrow[F=3,n_H=1]{} \frac{1}{16\pi^2}\left(-\frac{19}{6}\right) \\ b_{g'} &= +\frac{1}{16\pi^2}\left[+\frac{20F}{9} + \frac{n_H}{6}\right] \xrightarrow[F=3,n_H=1]{} \frac{1}{16\pi^2}\left(+\frac{41}{6}\right) \end{aligned} \tag{7.197}$$

for $SU(3)$, $SU(2)$, and $U(1)$, respectively[†]. These are valid at momenta much larger than m_t and ν, and assume the existence of F fermion families and n_H Higgs doublets. For $F = 3$ and $n_H = 1$, both $SU(3)$ and $SU(2)$ are asymptotically free.

λ and the Yukawa couplings also run. At one-loop (see, e.g., Cheng et al., 1974; Gunion et al., 1990)

$$\begin{aligned} \frac{d\lambda(Q^2)}{d\ln Q^2} =& \frac{1}{32\pi^2}\Big[24\lambda^2 + 24\lambda h_t^2 - 24h_t^4 - 3\lambda\left(3g^2 + g'^2\right) \\ &+ \frac{3}{8}\Big(2g^4 + (g^2 + g'^2)^2\Big)\Big] \\ \frac{dh_t(Q^2)}{d\ln Q^2} =& \frac{1}{32\pi^2}\Big[9h_t^3 - h_t\Big(8g_s^2 + \frac{9}{4}g^2 + \frac{17}{12}g'^2\Big)\Big], \end{aligned} \tag{7.198}$$

where it is understood that the couplings on the r.h.s. are the running couplings at Q^2. The quantity in (7.196) is the low energy value $\lambda(\nu^2)$, while $h_t(\nu^2) \sim m_t/\nu$ is the t-quark Yukawa coupling defined in (7.46) on page 295 or in (7.54); we have neglected all of the other Yukawas. The running of h_t is due to vertex, t quark, and Higgs self-energy diagrams (for a scalar coupling there is no analog of the Ward-Takahashi identity described in Section

[†]In considering grand unified theories it is conventional to introduce the *GUT-normalized* $U(1)$ gauge coupling $g_1 = \sqrt{\frac{5}{3}}g'$, which has the coefficient $b_{g_1} = \frac{3}{5}b_{g'} \to \frac{1}{16\pi^2}\,(+\frac{41}{10})$.

2.12.1). Typical one-loop diagrams contributing to the running of λ are shown in Figure 7.31.

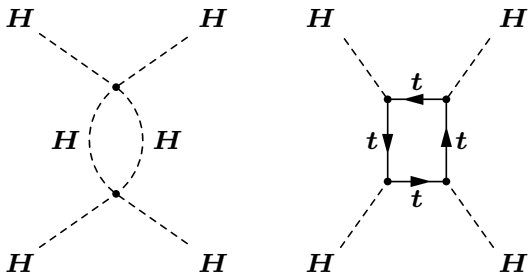

FIGURE 7.31
Typical diagrams contributing to the running of λ.

The first bound that we consider is the *triviality* upper limit on M_H (Cabibbo et al., 1979). From (7.196), $\lambda(\nu^2)$ is larger than unity for $M_H \gtrsim 350$ GeV, while $h_t(\nu^2) \sim 0.7$ for $m_t \sim 170$ GeV and the electroweak gauge coupling terms at low energy are small (Table 1.1). For large M_H one can therefore approximate the λ equation by the first term on the r.h.s., which is immediately solved to obtain

$$\lambda(Q^2) = \frac{\lambda(\nu^2)}{1 - \frac{3\lambda(\nu^2)}{4\pi^2} \ln \frac{Q^2}{\nu^2}}. \tag{7.199}$$

This diverges at the *Landau pole*

$$Q_{LP} = \nu e^{2\pi^2/3\lambda(\nu^2)}. \tag{7.200}$$

Presumably, it does not make sense for λ to diverge within the domain of validity of the theory[‡]. It suffices that Q_{LP} is larger than the scale Λ at which new physics sets in (and above which the RGE in (7.198) no longer apply). Requiring $Q_{LP} > \Lambda$ leads to the triviality limit

$$M_H < \left(\frac{2\sqrt{2}\pi^2}{3G_F \ln(\Lambda/\nu)} \right)^{1/2} \sim \begin{cases} \mathcal{O}(140) \text{ GeV}, \ \Lambda \sim M_P \\ \mathcal{O}(650) \text{ GeV}, \ \Lambda \sim 1500 \text{ GeV} \end{cases}, \tag{7.201}$$

where $M_P = G_N^{-1/2} \sim 1.2 \times 10^{19}$ GeV is the Planck scale. This limit is somewhat fuzzy, because the one-loop approximation is not valid when λ is large,

[‡]In the pure $\lambda H^4/4$ theory the only way for the one-loop RGE solution to remain finite for $Q^2 \to \infty$ would be to take $\lambda(\nu^2) = 0$, justifying the term triviality.

and in fact perturbation theory breaks down. However, it provides a reasonable estimate (as a function of the new physics scale) of how large a value of M_H is consistent with having a weakly coupled field theory. In particular, the observation of a SM-type Higgs at a mass scale much larger than 200 GeV would have strongly suggested that new physics sets in at a rather low scale. A more detailed evaluation including two-loop effects and the neglected terms in (7.198) is shown in Figure 7.32. One finds that $M_H \lesssim 180$ GeV for $\Lambda \sim M_P$, while $M_H \lesssim 700$ GeV for $\Lambda < 2M_H$. (It would not make much sense to consider an elementary Higgs field for a lower Λ.) The latter upper bound can be justified by non-perturbative lattice calculations (Hasenfratz et al., 1987; Kuti et al., 1988; Luscher and Weisz, 1989), which suggest an absolute upper limit of $650 - 700$ GeV.

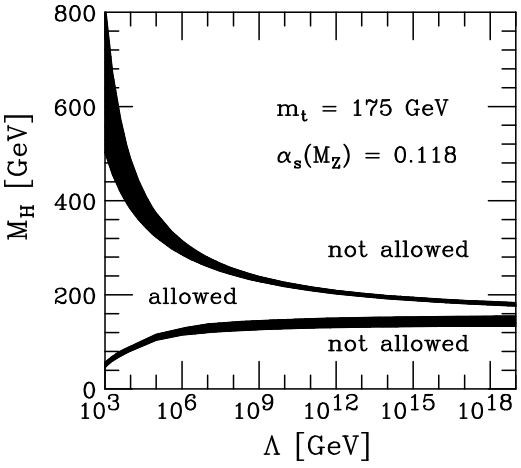

FIGURE 7.32
Theoretical limits on the SM Higgs mass as a function of the scale Λ at which new physics enters. The upper limit is from the absence of a Landau pole below Λ, while the lower limit is from vacuum stability. Reprinted with permission from (Hambye and Riesselmann, 1997).

There is also a lower limit on the Higgs mass from vacuum stability (e.g., Cabibbo et al., 1979; Altarelli and Isidori, 1994; Casas et al., 1996; Isidori et al., 2001; Degrassi et al., 2012; Buttazzo et al., 2013). To see this, consider the small λ limit of the first equation in (7.198). If we keep only the (dominant)

h_t^4 term[§], and also treat h_t as a constant, then one finds

$$\lambda(Q^2) \sim \lambda(\nu^2) - \frac{3h_t^4}{4\pi^2} \ln \frac{Q^2}{\nu^2}, \tag{7.202}$$

which goes negative at Q^2 for which

$$\lambda(\nu^2) = \frac{3h_t^4}{4\pi^2} \ln \frac{Q^2}{\nu^2}, \qquad M_H^2 = \frac{3h_t^4}{\sqrt{2}\pi^2 G_F} \ln \frac{Q}{\nu}. \tag{7.203}$$

A negative λ within the domain of validity of the theory would suggest an unstable vacuum, so we have a lower limit on $\lambda(\nu^2)$ and M_H^2 coinciding with the terms on the r.h.s. in (7.203) for $Q = \Lambda$. In particular, $M_H \gtrsim 85$ GeV for $\Lambda = 1500$ GeV. For large Λ it is not valid to neglect the running of h_t. One needs to integrate the coupled equations, include two-loop effects, and include loop contributions to the effective potential in addition to those in $\lambda(Q^2)$. Typical results are shown as a function of Λ in Figure 7.32. Combining the triviality and vacuum stability limits, M_H is constrained to the rather limited range $130 - 180$ GeV for $\Lambda = M_P$, with a somewhat larger range for smaller Λ. The lower limit is weakened somewhat (to around 115 GeV for $\Lambda = M_P$) if one allows a sufficiently long-lived (i.e., longer than ∼13.8 Gy, the age of the Universe) metastable vacuum (Casas et al., 1996; Isidori et al., 2001).

These limits do not apply in the minimal supersymmetric extension of the SM (the MSSM), because λ is not an independent parameter and there are additional contributions to the RGE. It is interesting that there is a complementary *upper* limit of ~ 130 GeV on the lightest Higgs scalar in the MSSM (increasing to ~ 150 GeV in extensions of the MSSM), which is close to the SM vacuum stability lower bound for most values of Λ. The observation of a Higgs much heavier or lighter than 130 GeV would have helped distinguish between the SM and supersymmetry, but the observed 125 GeV is inconclusive and somewhat challenging for both.

Tree Unitarity and the Equivalence Theorem

Another theoretical upper limit is based on the (tree-level) unitarity for $W^+W^- \to W^+W^-$ scattering and related processes such as ZZ, ZH, and HH scattering (Lee et al., 1977) (cf. the discussions of unitarity breakdown in high energy $\nu_e e \to \nu_e e$ and $e^+e^- \to W^+W^-$ scattering in Section 6.1). The potential difficulty involves the longitudinal polarization states for the W or Z, which dominate in high energy processes since the polarization vector $\epsilon_\mu(\vec{k}, 3) \sim k_\mu / M_{W,Z}$ grows with k at high energy. The amplitude for $W_L^+W_L^- \to W_L^+W_L^-$ (the subscript indicates longitudinal) is approximately

$$M = -i\sqrt{2}G_F M_H^2 \left(\frac{s}{s - M_H^2} + \frac{t}{t - M_H^2} \right) \tag{7.204}$$

[§]Lower limits that would have been relevant for a much lighter t quark are reviewed in (Gunion et al., 1990).

for $s, M_H^2 \gg M_W^2$, with the relevant diagrams shown in Figure 7.33. (We have ignored smaller terms which vanish for $g, g' \to 0$.) If one takes $M_H \to \infty$ this grows linearly with s, leading to violation of S-wave unitarity (Appendix C) at $\sqrt{s} \sim (16\pi\sqrt{2}/G_F)^{1/2} \gtrsim 2.4$ TeV, analogous to the problem in (6.6) on page 241 for $\nu_e e \to \nu_e e$ scattering in the Fermi theory. This illustrates why the existence of the Higgs (or some alternative form of spontaneous symmetry breaking) is essential to the consistency of the theory, since taking $M_H \to \infty$ is equivalent to removing it from the theory. However, there are problems even for finite M_H. It is straightforward to show (Lee et al., 1977; Gunion et al., 1990) that the S-wave amplitude obtained from (7.204) grows with M_H^2 for $s \gg M_H^2$, i.e.,

$$a_0 = -\frac{G_F M_H^2}{4\pi\sqrt{2}}, \tag{7.205}$$

where a_0 is the S-wave projection of the amplitude $T = -iM$, as defined in (C.5) and (C.7). The unitarity condition $|a_0| < 1$ then leads to an upper limit on M_H. This can be strengthened somewhat by considering the coupled channel analysis and a more precise unitarity constraint, leading to the unitarity bound

$$M_H \leq \left(\frac{4\pi\sqrt{2}}{3G_F}\right)^{1/2} \sim 700 \text{ GeV}, \tag{7.206}$$

which is comparable to the lattice version of the triviality bound.

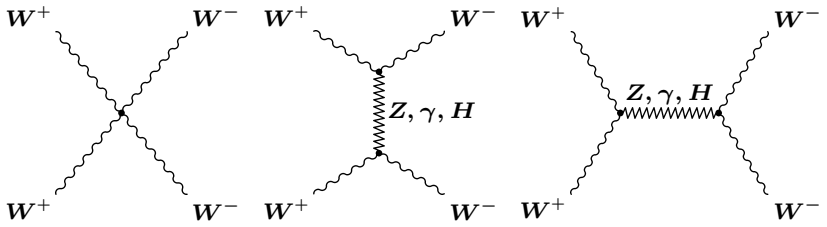

FIGURE 7.33
Tree-level diagrams for $W^+W^- \to W^+W^-$. The zigzag lines can represent a Z, γ or H.

Of course, (7.206) is based on the tree-level amplitude, and unitarity only applies rigorously to the full amplitude. One should therefore interpret (7.206) as the condition for a weakly coupled (perturbative) Higgs and gauge self-interaction sector, for which higher-order corrections to the amplitude are not expected to be important. Conversely, a violation of (7.206), or the nonobservation of a Higgs below this scale, would have suggested that spontaneous symmetry breaking is associated with a strongly coupled Higgs sector

or some strong coupling alternative to the elementary Higgs mechanism. This would presumably be manifested by enhanced WW cross sections at high energy (Chanowitz and Gaillard, 1985) and effects such as WW (bound state) resonances.

In Section 7.2.1 we applied the Kibble transformation to the Higgs doublet following SSB to go to the unitary gauge, in which it is manifest that the Goldstone bosons are eaten to become the longitudinal degrees of freedom of the $W^\pm$ and Z. We also saw above that amplitudes involving the W and Z at high energy are dominated by their longitudinal components. It is therefore not surprising that such high energy amplitudes can be calculated more easily in terms of the original Goldstone degrees of freedom using the *equivalence theorem* (Lee et al., 1977). (More rigorous discussions in more general gauges and including higher-order effects are given in (Chanowitz and Gaillard, 1985; Chanowitz et al., 1987).) We will illustrate this with a simple example, using the expressions (7.85) on page 306 for the Higgs doublet ϕ and (7.88) for the Higgs potential $V(\phi)$ in an R_ξ gauge, in which H is the physical Higgs field, and $w^\pm$ and z are the Goldstone degrees of freedom that disappear in the unitary gauge. (The gauge and Yukawa interactions for ϕ are also given in Section 7.2.4.) The equivalence theorem states that amplitudes involving high energy longitudinal Z's and W's can be obtained by the much simpler calculation of the corresponding amplitudes involving z and $w^\pm$. As a simple example, the $w^+w^- \to w^+w^-$ amplitude is given at tree-level by the four-point $w^+w^-w^+w^-$ vertex derived from (7.88), and by H exchange in the s and t channels. One finds

$$\begin{aligned} M &= -4i\lambda + (-2i\lambda\nu)^2 \left[\frac{i}{s-M_H^2} + \frac{i}{t-M_H^2}\right] \\ &= -2i\lambda \left[\frac{s}{s-M_H^2} + \frac{t}{t-M_H^2}\right], \end{aligned} \tag{7.207}$$

which reproduces (7.204) after using (7.196).

7.5.2 Higgs Properties, Searches, and Discovery

The Higgs interaction vertices are displayed in Figure 7.3 on page 293. They are always proportional to the mass of a fermion or to mass-squared for a boson, making the Higgs difficult to produce or detect in processes involving light particles. Here we consider searches for a relatively heavy ($M_H \gtrsim \mathcal{O}(10\text{ GeV})$) Higgs boson. Searches for lighter Higgs in nuclear physics, meson decays, etc., are described in (Gunion et al., 1990).

Higgs Production

There are a number of production mechanisms for the Higgs at hadron colliders, some in association with other particles, as indicated in Figure 7.34. The gluon fusion mechanism $GG \to H$, which proceeds via a virtual t-quark loop,

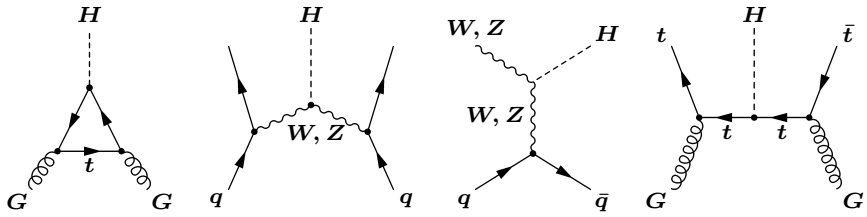

FIGURE 7.34
Representative Higgs production diagrams at a hadron collider, including gluon fusion (left), W or Z fusion (second left), and typical diagrams for associated production of WH, ZH, or $t\bar{t}H$.

has the largest cross section at both the Tevatron and the LHC, as shown in Figure 7.35. Observation of gluon fusion allows an indirect constraint on the $t\bar{t}H$ coupling, even for $M_H \ll 2m_t$. There are other modes with lower rates than gluon fusion, but with the advantage of allowing tagging on the associated particles. For example, the associated production of $W^{\pm}H$ or ZH (*Higgstrahlung*) is important. The ZH mode can be tagged by $Z \to \ell^-\ell^+$ with $\ell = e$ or μ, allowing a constraint on the ZH rate even for otherwise difficult modes such as $H \to b\bar{b}$ or for (non-standard) Higgs decays into unobserved particles. $WH \to \nu\ell H$ and $ZH \to \nu\bar{\nu}$ have even larger rates. Vector boson fusion ($W^+W^- \to H$ or $ZZ \to H$ with the W or Z radiated from a q or $\bar{q}$), has the second highest rate at the LHC and is associated with two hard jets. Associated $t\bar{t}H$ production is also important at the LHC. QCD (and electroweak) radiative corrections can be large. This is especially true for gluon fusion, where they are of $\mathcal{O}(100\%)$ at the LHC. They are described in the reviews and summarized in (Heinemeyer et al., 2013). The various production cross sections, including higher-order corrections, are shown for pp collisions as a function of $\sqrt{s}$ in Figure 7.36.

The dominant production mechanism in e^-e^+ at lower energies (e.g., LEP) is through associated Z production (Higgstrahlung), $e^-e^+ \to Z \to ZH$, analogous to the third diagram in Figure 7.34. At higher energies, W fusion, $e^-e^+ \to \nu_e W^-W^+\bar{\nu}_e \to \nu_e\bar{\nu}_e H$, (analogous to the second diagram in Figure 7.34) dominates because the cross section scales as $\ln(s/M_H^2)$ rather than $1/s$. Z fusion, $e^-e^+ \to e^-e^+H$, is cleaner than W fusion, but the cross section is an order of magnitude smaller. Smaller still is the cross section for $e^-e^+ \to t\bar{t}H$. However, this is dominated by the radiation of the Higgs from the t or $\bar{t}$ produced in $e^-e^+ \to t\bar{t}$ and could allow the determination of the $t\bar{t}H$ coupling in a future high energy collider. The predicted ZH and $\nu_e\bar{\nu}_e H$ cross sections are shown for several energies of possible future e^-e^+ colliders in Figure 7.37.

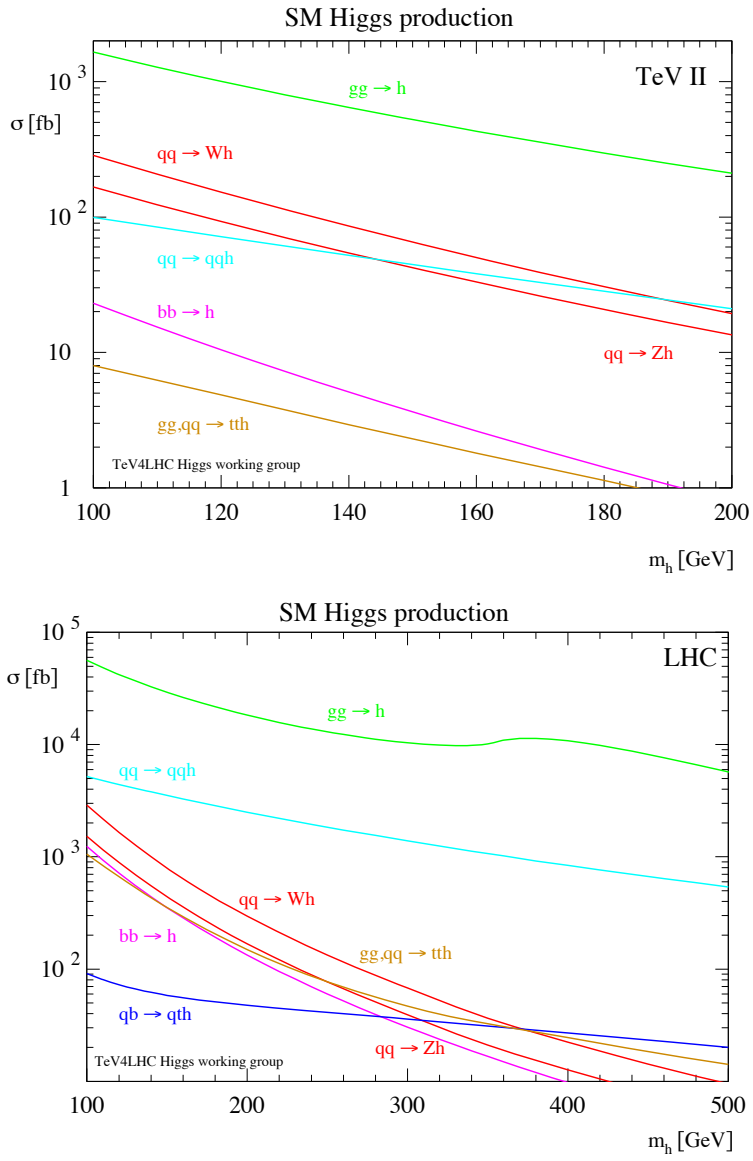

FIGURE 7.35
Higgs production cross sections at the Tevatron (1.96 GeV) and LHC (14 TeV) as a function of M_H, from (Aglietti et al., 2006).

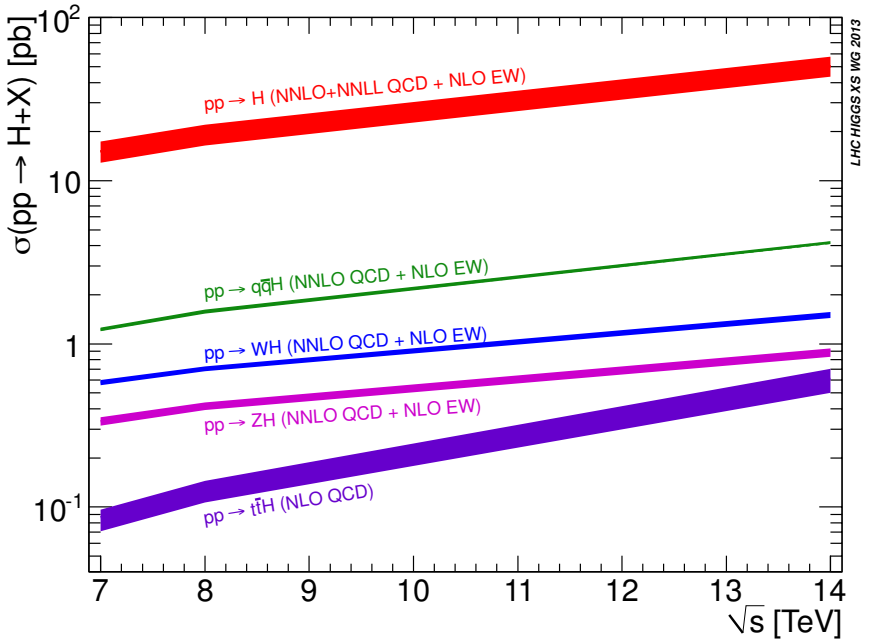

FIGURE 7.36
Production cross sections for a 126 GeV Higgs at the LHC as a function of $\sqrt{s}$, from the LHC Higgs Cross Section Working Group, `https://twiki.cern.ch/twiki/bin/view/LHCPhysics/CrossSections`.

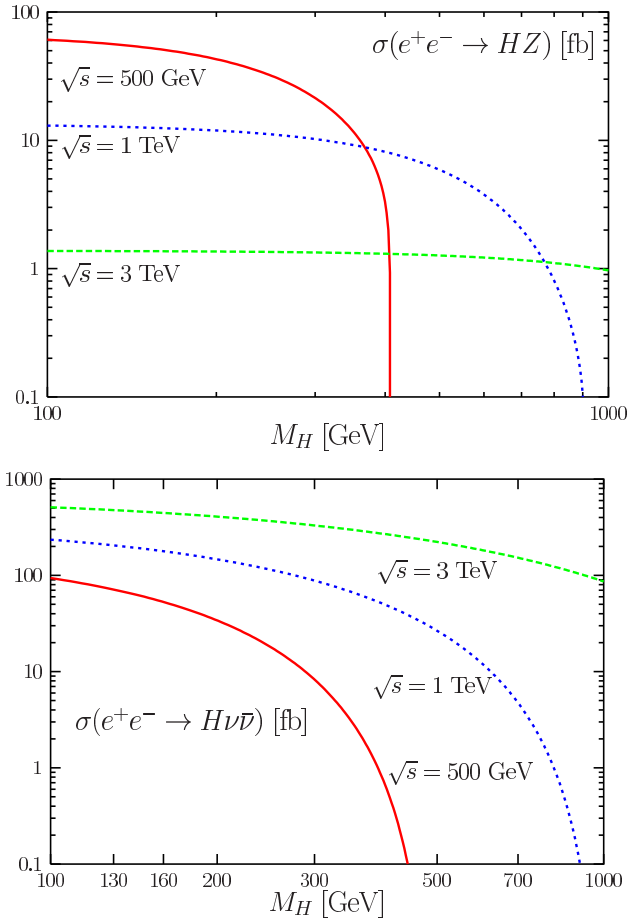

FIGURE 7.37
Cross sections for $e^-e^+ \to ZH$ (Higgstrahlung) and $\nu\bar{\nu}H$ (W fusion) at $\sqrt{s}$ = 500 GeV, 1 TeV, and 3 TeV, from (Djouadi, 2008a).

Higgs Decays

The standard model expectations for the various Higgs decay modes, including the details of the QCD and electroweak radiative corrections, are reviewed in (Djouadi, 2008a; Denner et al., 2011; Olive et al., 2014; Almeida et al., 2014; Lepage et al., 2014; Englert et al., 2014).

The predicted Higgs decay branching ratios are shown as a function of M_H in Figure 7.38. For large M_H, the decays $H \to W^+W^-$ and $H \to ZZ$ dominate. The cleanest signature in this case would be for the "golden" mode $H \to ZZ \to 4\ell$, but this is suppressed by the low leptonic branching ratios. The chains $H \to WW \to q\bar{q}\ell\nu$ and $H \to ZZ \to q\bar{q}\ell\bar{\ell}$ would therefore also be critical. Below the WW threshold, down to ~ 135 GeV, the decay WW^*, where W^* is off-shell, dominates, and ZZ^* is also important. For still lower masses $H \to b\bar{b}$ has the largest branching ratio. However, this mode is difficult at hadron colliders because of the very large QCD background, especially at the LHC. Thus, a Higgs produced by gluon fusion would be unobservable in $b\bar{b}$. The most promising light Higgs channels at the LHC are $H \to \gamma\gamma$, which proceeds at one-loop, and $H \to ZZ^* \to 4\ell$. These have very small branching ratios, but have clean signatures and lower backgrounds than the other modes, and in fact these turned out to be the discovery channels. Other modes with significant branching ratios for a light Higgs include GG, $\tau^+\tau^-$, and $c\bar{c}$. Associated productions of the Higgs with W, Z, or $t\bar{t}$, as well as vector boson fusion with hard forward quark jets, provide powerful additional handles, e.g., allowing the observation of $H \to b\bar{b}$ at hadron colliders.

The partial Higgs decay widths into fermions are

$$\Gamma(H \to f\bar{f}) = C_f \frac{G_F m_f^2}{4\sqrt{2}\pi} \beta_f^3 M_H, \tag{7.208}$$

where $\beta_f = (1 - 4m_f^2/M_H^2)^{1/2}$ is the fermion velocity and $C_f = 1$ (leptons) or 3 (quarks) is the color factor. The dominant QCD corrections for quarks are included by evaluating the running masses at M_H^2, e.g., $m_b((100\text{ GeV})^2) \sim 3$ GeV, reducing the width from the leading order expression. There are additional (smaller) corrections, e.g., from vertex diagrams. These fermionic widths are very small (except $H \to t\bar{t}$ for a very heavy H). For example, $\Gamma(b\bar{b})/M_H \sim 2 \times 10^{-5}$, so that $\Gamma(b\bar{b}) \sim 2$ MeV for $M_H = 100$ GeV. The partial widths for on-shell W^+W^- or ZZ are

$$\Gamma(H \to VV^\dagger) = \delta_V \frac{G_F}{16\sqrt{2}\pi} (1 - x_V)^{1/2} \left(1 - x_V + \frac{3}{4}x_V^2\right) M_H^3, \tag{7.209}$$

where $\delta_W = 2$, $\delta_Z = 1$, and $x_V = 4M_V^2/M_H^2$. The partial width grows as M_H^3. This is because for $M_H \gg M_V$ the decay is dominated by the longitudinal vector states, and their polarization vectors are of order M_H/M_V (see Problem 7.16). Asymptotically,

$$\Gamma(H \to W^+W^- + ZZ)/M_H \sim \frac{1}{2}\left(\frac{M_H}{1\text{ TeV}}\right)^2, \tag{7.210}$$

so a heavy Higgs is expected to be very broad, while a light one is very narrow. The partial widths for virtual decays, $\Gamma(H \to VV^*)$ are given, e.g., in (Gunion et al., 1990; Djouadi, 2008a).

The decays $H \to \gamma\gamma$, $Z\gamma$, and GG occur at one-loop. At tree level

$$\Gamma(H \to GG) \sim \frac{G_F \alpha_s^2 M_H^3}{36\sqrt{2}\pi^3} \tag{7.211}$$

for $M_H \ll 2m_t$, from the top-loop diagram in Figure 7.39, with α_s evaluated at M_H. There is a very large QCD correction. At one-loop order (Djouadi et al., 1991) the rate is enhanced by $1 + \delta\alpha_s/\pi$, where $\delta = 95/4 - 7N_f/6$, i.e., an increase of $\sim 70\%$ for $N_f = 5$. The GG decay is of course difficult to observe at a hadron collider but can be probed indirectly by measuring the GG fusion rate. Similarly, the $H \to \gamma\gamma$ decay is dominated by the W and top loops in Figure 7.39, which partially cancel. For $M_H \ll 2M_W$, the SM prediction is

$$\Gamma(H \to \gamma\gamma) \sim \frac{G_F \alpha^2 M_H^3}{128\sqrt{2}\pi^3} \left| -7 + \frac{4}{3} C_t q_t^2 \right|^2 , \tag{7.212}$$

where the first term is from the W, while the $4C_t q_t^2/3 = 16/9$ is from the top. See the reviews for corrections for finite M_H, higher order corrections, and $\Gamma(H \to Z\gamma)$.

Precision Electroweak Constraints

As described in Section 7.3.4, the precision electroweak data depend logarithmically on M_H due to the loop contributions to the gauge self-energies, shown in Figure 7.17 on page 335. These favor a relatively low value¶, $60 < M_H < 127$ GeV at 90% cl, with a central value $M_H = 89^{+22}_{-18}$ GeV (Olive et al., 2014). The allowed region in the m_t-M_H plane is shown in Figure 7.40.

Direct Searches at Colliders

The Higgs was searched for directly at LEP, through the Higgstrahlung process $e^- e^+ \to Z \to ZH$, which probes the ZZH vertex in Figure 7.3. At LEP 1, the s-channel Z was on-shell and the final one virtual, while at LEP 2, the s-channel Z was virtual. Various combinations of final states were searched for, including $H \to b\bar{b}$ or $\tau^-\tau^+$ and $Z \to q\bar{q}, \ell^-\ell^+$, or $\nu\bar{\nu}$. The LEP experiments were able to exclude a SM Higgs with mass below 114.4 GeV at 95% cl (Barate et al., 2003; Olive et al., 2014). There were hints of a signal at ~ 115 GeV, but this was inconclusive. As seen in Figure 7.40 there is some tension between the precision fits and the direct lower limit, but no real conflict. LEP 2 also obtained limits on possible Higgs-like states with masses below 114.4 GeV but with reduced rates compared to the SM expectation, as would be expected in some extended models as discussed below.

¶These results supersede those in Section 7.3.6.

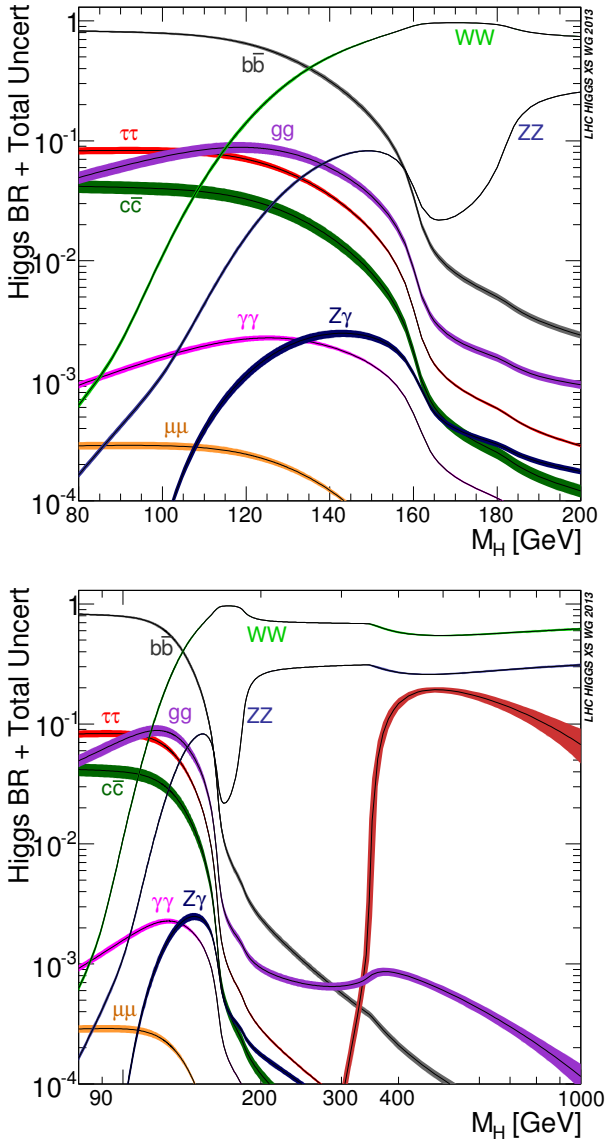

FIGURE 7.38
Branching ratios for the principal SM Higgs decays as a function of M_H, including theoretical uncertainties (Denner et al., 2011), from (Heinemeyer et al., 2013). The unlabeled curve in the lower plot (third highest for very large M_H), is for $t\bar{t}$.

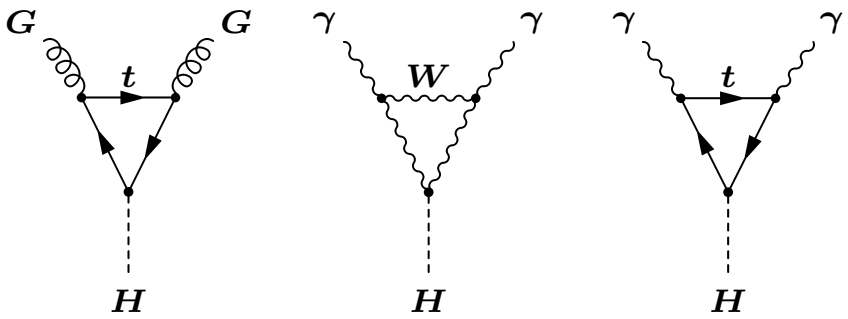

FIGURE 7.39
Diagrams for the loop-induced decays $H \to GG$ and $H \to \gamma\gamma$.

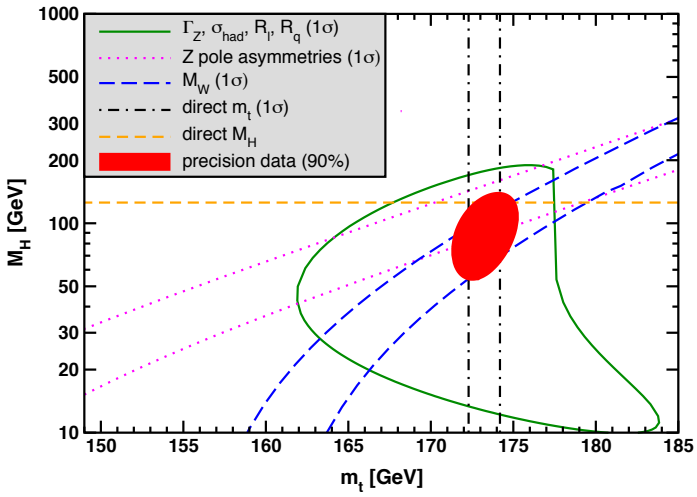

FIGURE 7.40
1σ allowed regions in M_H vs m_t and the 90% cl global fit region from precision data, compared with value $M_H \sim 125.6$ GeV (dashed yellow line) from ATLAS and CMS. Plot courtesy of the Particle Data Group (Olive et al., 2014).

The CDF and D0 experiments at the Tevatron (see, e.g., (Bernardi and Herndon, 2014)) could probe to higher values of the SM Higgs mass once they had acquired sufficient integrated luminosity. Initially, they were mainly sensitive to $H \to W^+W^-$ in the mass range $160-170$ GeV near or just above threshold. With increased luminosity their sensitivity increased and they could search for lower Higgs masses via associated VH production ($V = W$ or Z), with $H \to b\bar{b}$ (the Tevatron $b\bar{b}$ background is not so large as that at the LHC). By the time the Tevatron ceased running in 2012 the collaborations had searched for the SM Higgs in the range 90-200 GeV in the decay modes $b\bar{b}$, W^+W^-, ZZ, $\tau^-\tau^+$, and $\gamma\gamma$ at $\sqrt{s} = 1.96$ TeV with integrated luminosities $L = \int \mathcal{L}dt$ up to 10 fb^{-1}, taking into account all of the production mechanisms in Figure 7.34. Their combined analysis (Aaltonen et al., 2013) excluded a SM Higgs in the mass ranges $90 - 109$ and $149 - 182$ GeV, and observed a broad excess of events (mainly $Vb\bar{b}$) from 115-140 GeV. Taking resolution into account this was consistent with the LHC observations and with a SM Higgs, with a local significance[‖] of 3.0σ for $M_H = 125$ GeV.

The Higgs Discovery and Properties

Because of the higher energy (and therefore cross sections), and eventually the larger integrated luminosity, the LHC experiments ATLAS and CMS were sensitive to a SM or MSSM Higgs over the entire relevant mass range (Bernardi and Herndon, 2014). Each of the two experiments obtained $L \sim 5$ fb^{-1} at $\sqrt{s} = 7$ TeV during 2011 and ~ 20 fb^{-1} at $\sqrt{s} = 8$ in 2012. The 7 TeV data, combined with the earlier collider experiments, was sufficient to exclude a light SM Higgs below 116 GeV or a heavy SM Higgs between 127 and 600 GeV, leaving only a relatively small window (which was also in the range expected from precision electroweak measurements). By the end of 2011 both experiments reported significant excesses around 120-126 GeV in both the $\gamma\gamma$ and 4ℓ, $\ell = e^{\pm}$ or $\mu^{\pm}$ channels.

By the summer of 2012 there were sufficient statistics for CMS (Chatrchyan et al., 2012, 2013, 2014) and ATLAS (Aad et al., 2012, 2013b,a) to announce $> 5\sigma$ discoveries of a Higgs-like particle of mass $\sim (125-126)$ GeV. The most significant channels were again $\gamma\gamma$ and 4ℓ (from $H \to ZZ^* \to 4\ell$), for which there is the best mass resolution (see Figures 7.41 and 7.42). The lineshape analyses[**] for these combined modes yielded $M_H \sim 1.25 \pm 0.6$ GeV (ATLAS)[††]

[‖]The local significance is for a definite M_H, while the lower global significance takes into account the look-elsewhere effect, i.e., that a statistical fluctuation of the background could have occurred anywhere in a given mass range.

[**]Important subsequent updates include (Aad et al., 2014a) (ATLAS) and (Khachatryan et al., 2014c) (CMS). The most recent results are available from the CMS and ATLAS public websites:
`https://twiki.cern.ch/twiki/bin/view/CMSPublic/PhysicsResultsHIG`
`https://twiki.cern.ch/twiki/bin/view/AtlasPublic/HiggsPublicResults`.

[††]The ATLAS mass values from $\gamma\gamma$ and 4ℓ, $\sim 126.8 \pm 0.7$ and 124.3 ± 0.8, respectively,

and 125.7 ± 0.4 GeV (CMS).

The rates for H production and decay into a specific final state a are proportional to $\sigma_H B(H \to a)$ where σ_H is the production cross section and $B(H \to a) = \Gamma(H \to a)/\Gamma_H$ is the branching ratio into a. At a hadron collider one can most cleanly measure the relative branching ratios into two different final states. The branching ratios $B(H \to a)$ themselves can be obtained if σ_H is known independently from a theoretical calculation or by tagging some inclusive production mode, such as vector boson fusion or by WH or ZH, with W or $Z \to$ jets, $Z \to 2\ell$, or $Z \to b\bar{b}$. The $B(H \to a)$ can also be obtained if the relative rates for all significant decay modes[‡‡] are known, using the constraint that $\sum_a B(H \to a) = 1$.

Determination of the more interesting absolute widths $\Gamma(H \to a)$ requires an independent determination of the total width Γ_H. CMS obtained an upper limit of 6.9 GeV at 95% c.l. on Γ_H from the lineshape. This is very much larger than the intrinsic width of ~ 4 MeV expected in the SM, and is presumably due almost entirely to the experimental resolution. CMS subsequently obtained a much more stringent limit $\Gamma_H < 22$ MeV at 95% c.l. (Khachatryan et al., 2014a) indirectly by comparing the $H \to ZZ^*$ rates on-shell and off-shell, making use of the Breit-Wigner energy dependence in (F.2) on page 561. This is still considerably larger than the SM expectation, however. A precise determination of Γ_H will probably require a measurement of the $e^-e^+ \to ZH$ rate at a future e^-e^+ collider (to obtain the ZZH vertex and therefore $\Gamma(H \to ZZ^*)$), combined with $B(H \to ZZ^*)$.

CMS and ATLAS* also found evidence for a broad enhancement in 2ℓ, presumably from $H \to WW^* \to \ell\nu\ell\nu$. The rates (production cross section times branching ratio) for $\gamma\gamma$, ZZ^*, and WW^* are in good agreement with the SM Higgs interpretation[†], although the uncertainties are still high, $\mathcal{O}(20-30\%)$, as can be seen in Figure 7.43.

Decays of the Higgs-like particle into fermions are not so well established. However, preliminary results as of February 2014, based on the entire 2011-2012 data set, establish that $H \to \tau^-\tau^+$ and $VH \to Vb\bar{b}$ do indeed occur, with a combined significance of around 4σ per experiment, with the highest significance for $\tau^-\tau^+$. The rates are consistent with the SM, though the un-

differ by about 2.4σ. The discrepancy is not understood. A subsequent analysis reduced the effect to a less significant 2σ (Aad et al., 2014a).

[‡‡]As discussed below some scenarios beyond the standard model involve *invisible* (unobserved) decay modes that must also be included. Their rates can be constrained or observed by tagging.

*In December 2014 ATLAS reported the observation of $H \to WW^*$ in the dilepton channel at a significance of 6.1σ, with rates for both gluon and vector boson fusion consistent with the SM (Aad et al., 2014b).

[†]The initial results from both experiments yielded a $\gamma\gamma$ rate 50-60% higher than the SM expectation (though with large uncertainties), leading to considerable speculation concerning a deviation from the SM. However, the case for new physics was significantly weakened by subsequent results from CMS, which yielded a lower rate.

certainties are still quite large. There have also been upper limits established on decay modes such as $\mu^-\mu^+$ and $Z\gamma$. These are still well above the SM expectations.

Some beyond the standard model scenarios predict Higgs decay modes into invisible final states, such as MSSM neutralinos or *dark sector* candidates for dark matter, or into a pair of pseudoscalars in some models with extended Higgs sectors. These are constrained by tagged events such as Higgstrahlung or vector boson fusion, yielding limits of ∼(60-70)% on the branching ratio for $H \to$ invisible.

The various production mechanisms can be separated experimentally by tagging on the associated forward jets, Z, W, or t. As can be seen in Figure 7.44 the production rates are consistent with the SM expectations, though with quite large uncertainties.

From Figures 7.43 and 7.44 it is apparent that the production and decays of the Higgs-like particle are broadly consistent with the expectations for the SM Higgs. All of the available information has been combined in global analyses to test consistency with the SM in more detail and to constrain the magnitudes of possible deviations, e.g., (Giardino et al., 2014; Ellis and You, 2013; Belanger et al., 2013). One of the most fundamental properties of the SM Higgs boson is that its couplings are proportional to a power of mass, i.e., to $h_f \equiv m_f/\nu$ for fermion f, or to $h_V \equiv 2M_V^2/\nu$ for $V = W, Z$. This is indeed the case, as can be seen in Figure 7.45.

Another critical aspect is to determine the spin, parity, and charge conjugation quantum numbers J^{PC}. These are predicted to be 0^{++} for the SM Higgs, i.e., the couplings to fermions and vectors are proportional to $H\bar{\psi}\psi$ and $HV_\mu V^\mu$ (or $HV_{\mu\nu}V^{\mu\nu}$ at loop level), respectively. However, dynamical alternatives to the elementary Higgs mechanism often involve pseudoscalars, $J^{PC} = 0^{-+}$, which could be light (Eichten et al., 2012). A pseudoscalar P would couple like $P\bar{\psi}\gamma^5\psi$ and $PV_{\mu\nu}\tilde{V}^{\mu\nu}$, where $\tilde{V}^{\mu\nu} = \frac{1}{2}\epsilon^{\mu\nu\rho\sigma}V_{\rho\sigma}$. If a light pseudoscalar somehow had the appropriate coupling strengths it could mimic the SM Higgs. In principle, the Higgs-like particle could also have spin higher than 0.

The fact that the H decays to $\gamma\gamma$ implies that it has $\eta_C = +1$ (or that it is not a C eigenstate). It also implies[‡] that $J = 0, 1,$ or 2 under the plausible assumption of an S-wave decay. The $J^P = 0^+$ and 0^- cases can be distinguished by angular and invariant mass distributions in $H \to ZZ^* \to 4\ell$, and also by the threshold behavior of VH, e.g., (Bolognesi et al., 2012). The 4ℓ decays have allowed ATLAS and CMS to exclude a pure pseudoscalar at

[‡]According to the Landau-Yang theorem (Landau, 1948; Yang, 1950), which follows from rotational invariance and Bose statistics, a spin-1 particle cannot decay into two identical massless vectors. It can be evaded for off-shell, massive, or non-identical vectors, for processes that are mistaken for two photons, or if there are two decaying particles. It is therefore useful to exclude this possibility experimentally.

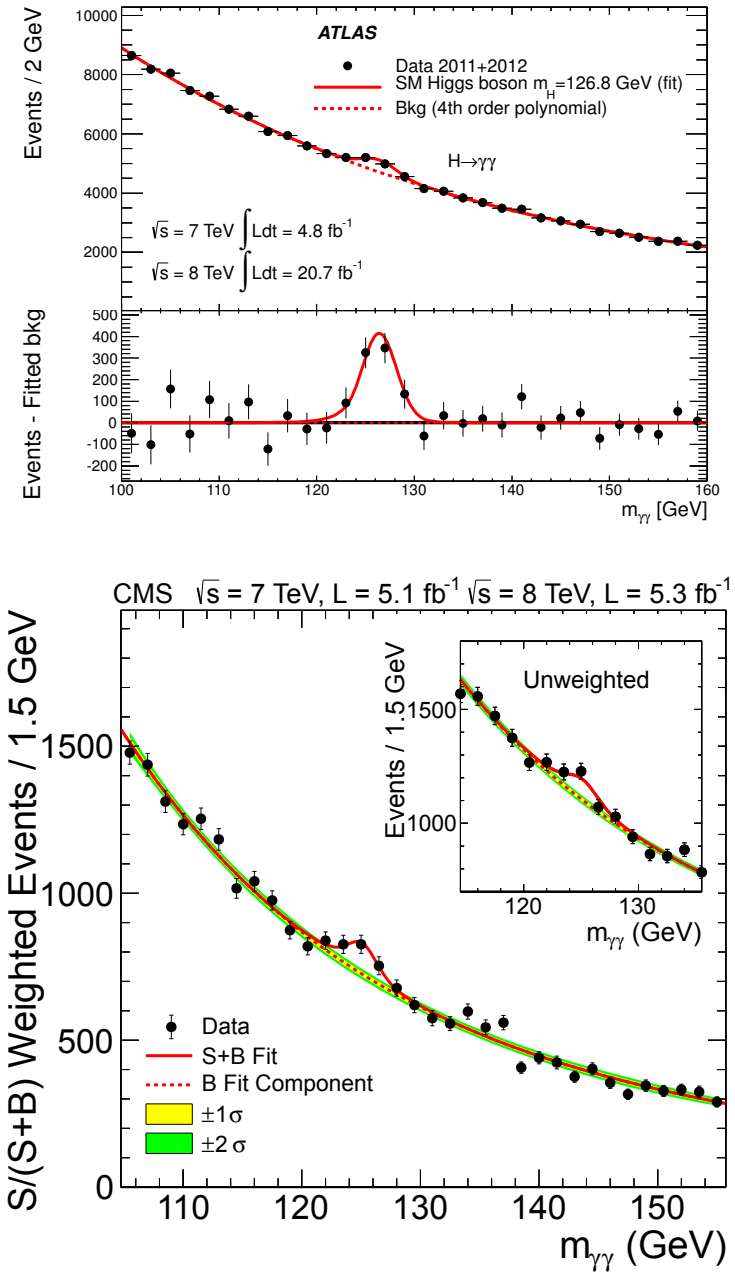

FIGURE 7.41
Diphoton mass spectra from ATLAS (Aad et al., 2013b) and CMS (Chatrchyan et al., 2013).

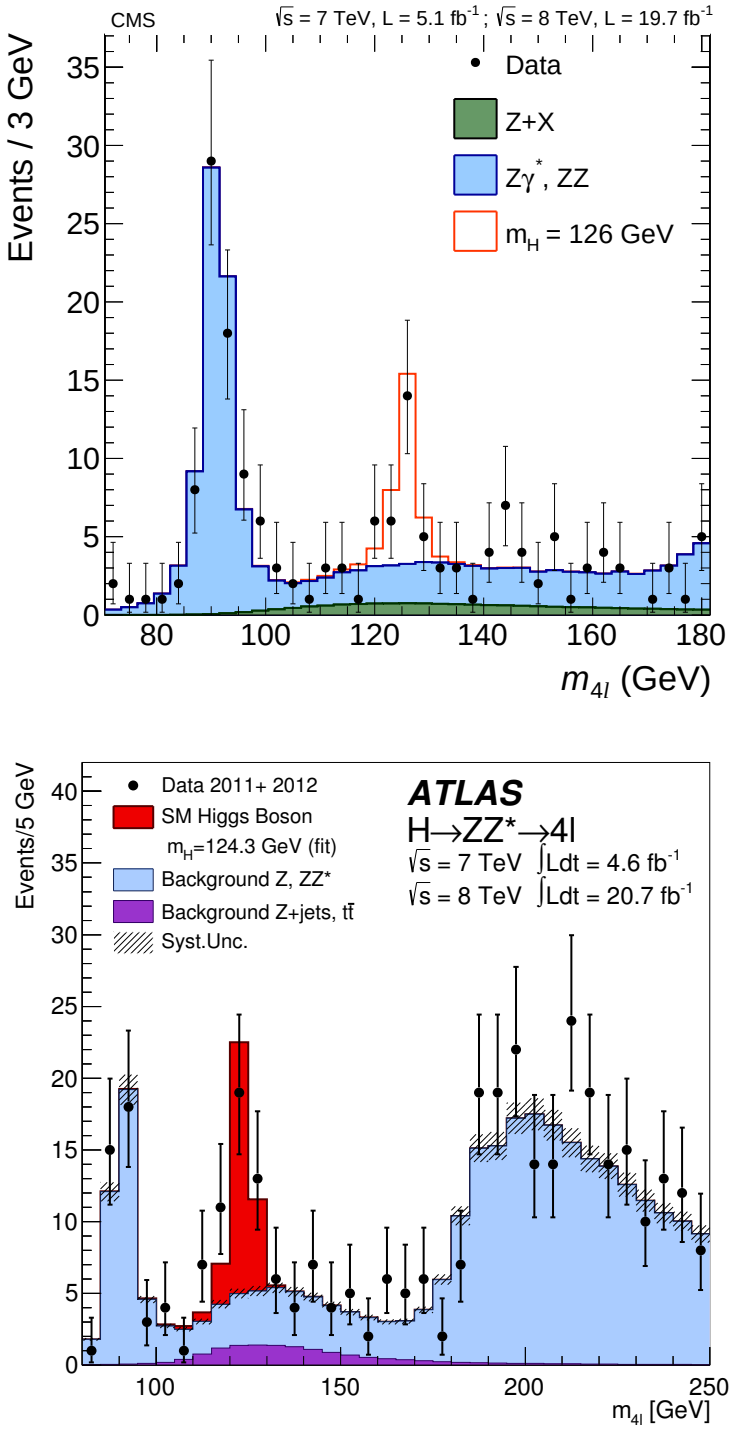

FIGURE 7.42
Four-lepton invariant mass distribution from CMS (Chatrchyan et al., 2014) and ATLAS (Aad et al., 2013b).

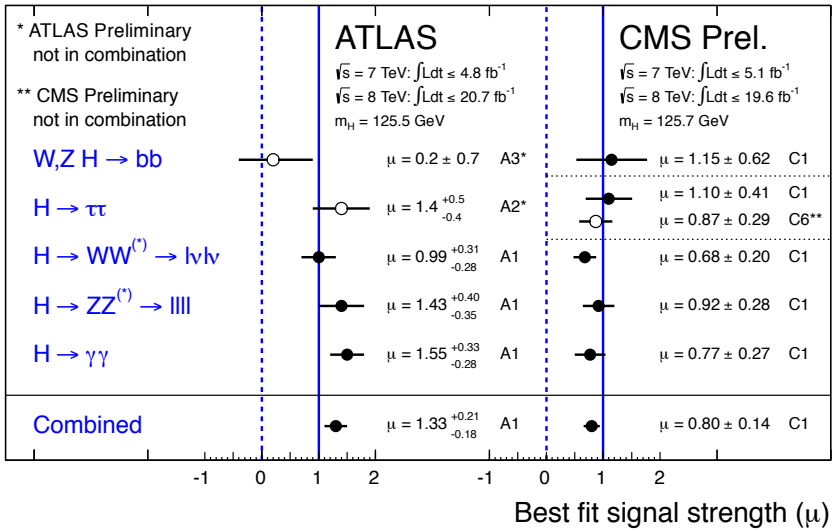

FIGURE 7.43
Signal strengths μ (ratio of observed rate to the expectation for a SM Higgs) for various decay modes for ATLAS and CMS, from (Olive et al., 2014).

better than 99% c.l. The 0^+ can be distinguished from $1^\pm$ and 2^+ in ZZ^*, WW^*, and $\gamma\gamma$. Most of these possibilities are now excluded[§] at $\gtrsim 98\%$ c.l.

Implications of the Higgs Discovery

The various observations described in the previous section leave little doubt that the observed state is either the SM Higgs, or something very similar to it. Assuming that it really is the SM Higgs, its relatively low mass implies some tension with the the vacuum stability considerations discussed in Section 7.5.1. A recent NNLO calculation of the effective potential and running couplings (Degrassi et al., 2012; Buttazzo et al., 2013) shows that for the observed parameters the quartic coupling $\lambda(Q^2)$ goes negative for Q around $10^{10} - 10^{12}$ GeV. See the Figure 7.46 (top). However, the decrease of λ slows for larger Q^2 due to cancellations, implying a metastable vacuum (with the lifetime longer than the observed age of the Universe). It is remarkable that the observed parameters imply that the SM vacuum lies in the narrow strip between instability and absolute stability[¶]. It should be reiterated that these

[§]See (Khachatryan et al., 2014b) for a recent CMS update.

[¶]The value $\lambda(M_P^2) = 0$ would be theoretically intriguing and would open the possibility that the Higgs is the inflaton of inflationary cosmology (Bezrukov et al., 2012; Salvio, 2013).

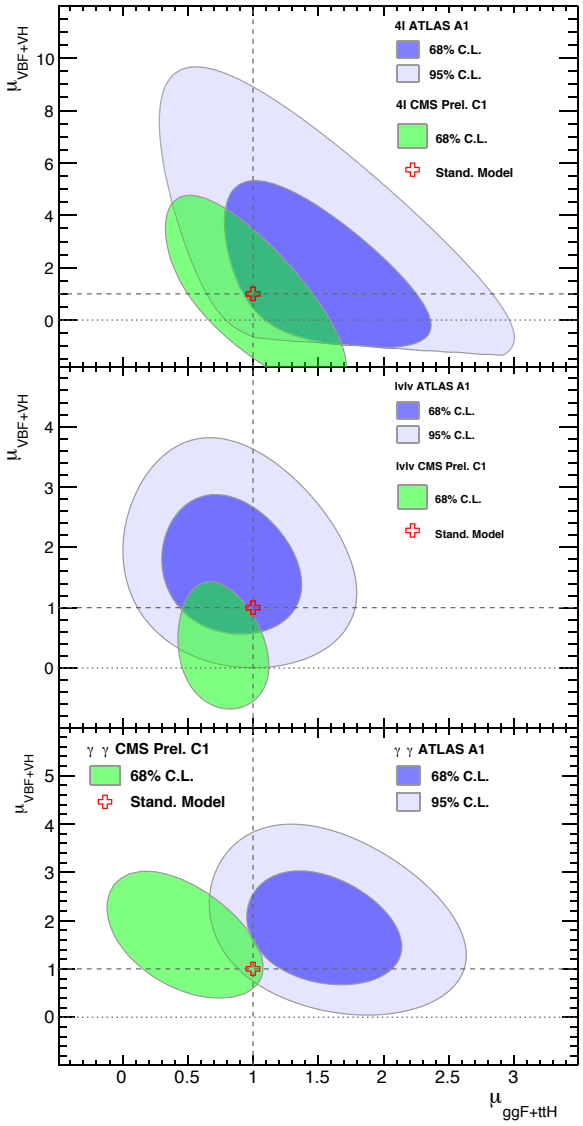

FIGURE 7.44
Allowed regions in the production rates (relative to the SM predictions) for (GG fusion $+t\bar{t}H$) vs (vector boson fusion $+VH$) from CMS and ATLAS for the 4ℓ, $\ell\nu\ell\nu$, and $\gamma\gamma$ final states, from (Olive et al., 2014).

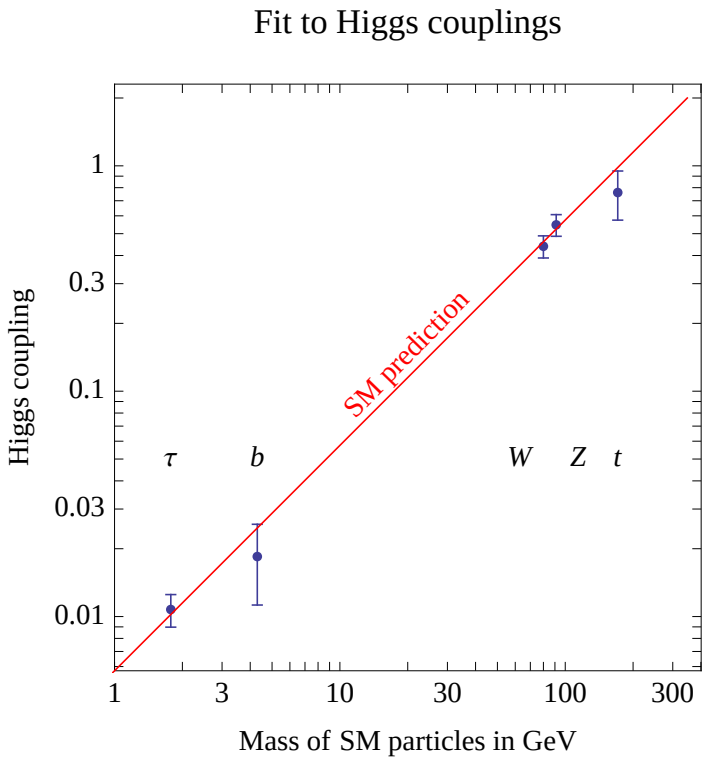

FIGURE 7.45
Plot of the tree-level Higgs couplings to fermions ($\sqrt{2}h_f$) and gauge bosons ($\sqrt{h_V/\nu}$) as a function of mass, from the global analysis in (Giardino et al., 2014).

considerations only apply if there is no new physics below the Planck scale M_P, or at least below the scale at which λ vanishes.

Extended Electroweak Symmetry Breaking Sectors

The observed Higgs-like particle is consistent with the SM Higgs. However, the measurements of its couplings still leave considerable room for deviations. These could be due either to extended sectors involving elementary Higgs fields or to the possibility that the Higgs sector is an effective theory describing underlying strong dynamics at a higher scale. Some of these extensions are motivated by the Higgs/hierarchy problem described in Section 8.1. This basically states that the Higgs mass-squared involves quadratically-divergent corrections of $\mathcal{O}(\lambda, g^2, h^2)\Lambda^2$ (see (8.2) on page 457), where Λ is the new physics scale. This implies that for $\Lambda \gg$ TeV there must be fine-tuned cancellations between the bare mass-squared and the corrections.

Many theories beyond the SM have extended Higgs sectors[‖], involving additional Higgs doublets (such as are required in supersymmetry) and/or Higgs fields transforming under different $SU(2)$ representations, such as singlets or triplets (for reviews, see Gunion et al., 1990; Djouadi, 2008b; Accomando et al., 2006; Barger et al., 2007; Djouadi et al., 2008; Djouadi and Godbole, 2009; Branco et al., 2012; Olive et al., 2014). Such additional multiplets allow new physical scalar particles, including extra electrically-neutral states, singly-charged states for additional doublets or triplets, and even doubly-charged states for $SU(2)$ triplets with $y = \pm 1$. Electrically neutral states may mix with the H (even for $SU(2)$ singlets), modifying the couplings of the mass eigenstates h_i. In some cases, there are two or more mass eigenstates with scalar couplings to fermions, and one or more with pseudoscalar (γ^5) couplings, and in other cases (involving CP violation) the scalars and pseudoscalars mix. In the MSSM, for example, there are two Higgs doublets. In the decoupling limit, in which the second Higgs doublet is much heavier than the first, there is little mixing and the lighter scalar has couplings essentially the same as those of the SM Higgs. However, there can be considerable mixing between the two scalars (and with the pseudoscalar if CP is violated) in the non-decoupling region, in which the new supersymmetric particles and second Higgs are relatively light.

An important consequence of mixing prior to the discovery of the Higgs-like particle was that the LEP 2 lower limit of 114.4 GeV could be weakened, e.g., because the strength of the ZZh_1 coupling could be reduced due to the mixing between two scalars or because the lightest scalar has new decay modes which are difficult to observe, such as into two light pseudoscalars (Chang et al., 2008). In the non-decoupling region of the MSSM, for example, the LEP 2

However, this case is excluded at better than 98% c.l. (Buttazzo et al., 2013).

[‖]We are using Higgs in the sense of any spin-0 color-singlet fields which are not forbidden by additional symmetries from mixing with the SM Higgs doublet.

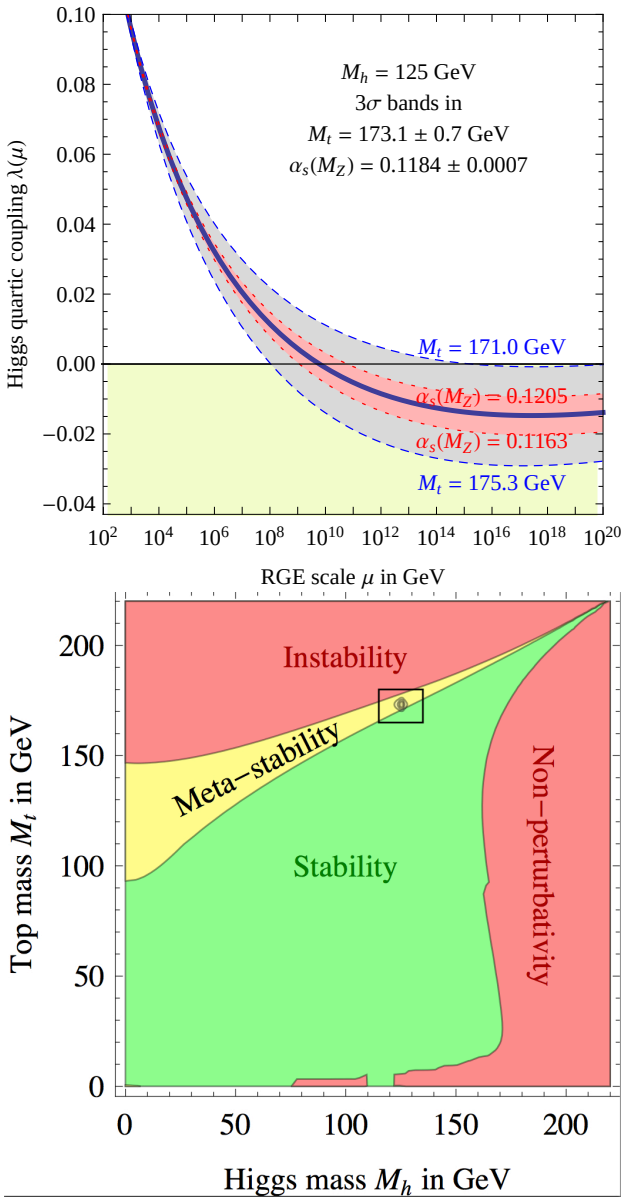

FIGURE 7.46
Top: The running of the quartic Higgs self-coupling for $M_H = 125$ GeV, from (Degrassi et al., 2012). The vacuum remains metastable for $\lambda(M_P^2) \gtrsim -0.05$. Bottom: Phase diagram for the standard model as a function of M_H and m_t, assuming that there is no new physics up to the Planck scale. From (Degrassi et al., 2012).

limit was weakened by the mixing effect (Heinemeyer et al., 2006, 2008; Barate et al., 2003), although this was partially compensated by a new search channel, $Z^* \to$ scalar + pseudoscalar. This will be further discussed in Chapter 8.

In addition to the implications for the Higgs spectrum and couplings, extended Higgs sectors can lead to flavor changing Higgs-fermion couplings (e.g., in non-supersymmetric two-doublet models in which both doublets couple to the same fermions), or to modifications to the ρ_0 parameter (i.e., to the M_W/M_Z relation) due to the VEVs of Higgs triplets or higher-dimensional representations (Problem 7.1) unless a custodial symmetry is somehow imposed. There are also new possibilities for explicit or spontaneous CP violation in the Higgs sector (with possible implications for baryogenesis (Barger et al., 2007)), and even the danger of the spontaneous violation of electric charge (Problems 7.3 and 7.4). Higgs singlets in extended models can also be dark matter candidates (Barger et al., 2009) or can serve as *portal* connecting the standard model fields to a dark matter sector (Schabinger and Wells, 2005; Patt and Wilczek, 2006).

Many of these possibilities have been reexamined in light of the discovery of the Higgs-like particle. In particular, there have been detailed studies of the lightest Higgs scalar in the decoupling limit of the MSSM (Hall et al., 2012; Draper et al., 2012; Degrassi et al., 2012; Carena et al., 2013; Hahn et al., 2014; Buchmueller et al., 2014). One of the primary motivations of supersymmetry is to solve the Higgs/hierarchy problem via cancellations of the Higgs mass quadratic divergences due to the SM particles against additional diagrams involving their superpartners. However, the MSSM immediately leads to another complication: it has already been commented in Section 7.5.1 that there is a theoretical upper limit of ~ 130 GeV on the mass of the lightest Higgs scalar in the MSSM, due to the fact that the analog of λ in the SM is given by gauge couplings. In fact, at tree level, the upper limit is actually M_Z. A larger M_H is possible due to loop corrections for large masses and/or mixings of the two scalar partners of the top quark (see (8.160) on page 499), but to achieve a mass as high as 125-126 GeV requires either very large stop masses in the multi-TeV range or very large mixing, as is illustrated in Figure 7.47. The large ratio of these scales to the electroweak scale ν, which is closely associated with the supersymmetry breaking parameters, requires cancellations that are possible but which appear rather unnatural (the little hierarchy problem). The theoretical upper limit of ~ 130 GeV on M_H is considerably weakened (to around 150 GeV) in extended supersymmetric models, especially in the singlet-extended models discussed in Section 8.2.6. Recent studies of these and other extended-Higgs models include (Frank et al., 2013; Craig et al., 2013; Baglio et al., 2014).

It is all possible that there are no elementary Higgs particles. For example, the symmetry breaking could be associated with the boundary conditions in a theory with extra dimensions of space-time (*Higgsless models*), for which there are no analogs of the Higgs field. Alternatively, electroweak symmetry breaking could be due to some sort of bilinear fermion condensate, as in

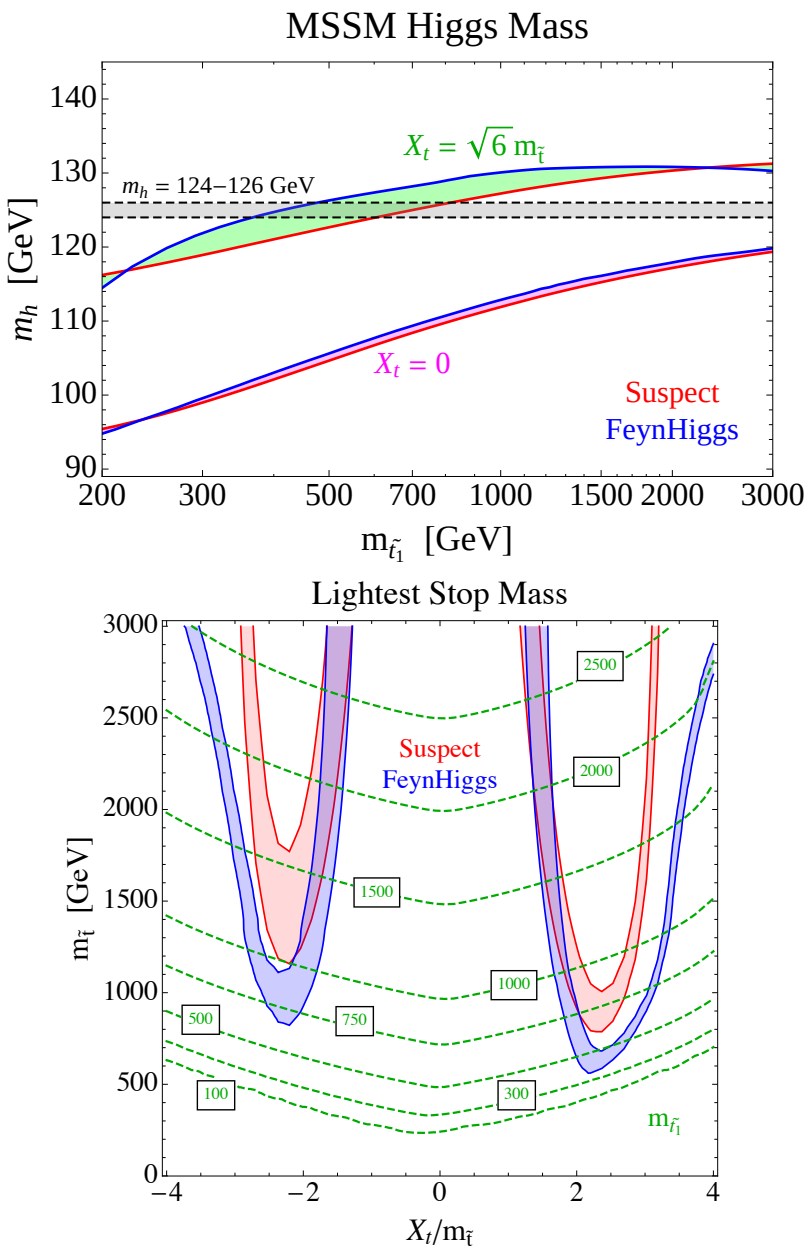

FIGURE 7.47

Top: lightest Higgs mass in the MSSM. Bottom: MSSM parameter regions that can accomodate a lightest Higgs scalar in the 124-126 GeV range, both from (Hall et al., 2012). X_t is the stop squark mixing parameter defined in (8.176) on page 503; $m_{\tilde{t}}$ is the soft stop mass, which is (here) assumed to be the same for both $\tilde{t}_L$ and $\tilde{t}_R$; and $m_{\tilde{t}_1}$ is the lighter stop eigenvalue. $X_t = 0$ and $X_t \sim \sqrt{6} m_{\tilde{t}}$ are the no-mixing and maximal-mixing scenarios discussed in Section 8.2.5. The packages Suspect and FeynHiggs are referenced in the Web Sites section at the end of this book.

the spontaneous breaking of the chiral symmetries in QCD (Section 5.7). Examples include (extended) technicolor and top-color. However, such models do not usually have a light 0^+ scalar that could imitate the SM Higgs. See Section 8.1 for a more detailed discussion.

More promising are composite Higgs models. Typically, these involve a more fundamental strongly-coupled sector at the $1-10$ TeV scale which (unlike technicolor) does not directly lead to electroweak symmetry breaking. However, the Higgs multiplet emerges as a composite state in a low-energy effective theory. A very attractive possibility is that, in the absence of electroweak or Yukawa couplings, all four Hermitian components of the Higgs doublet are the massless Goldstone bosons associated with a spontaneously broken global symmetry of the underlying theory. Turning on the electroweak couplings generates the Higgs potential, which in turn leads to $SU(2) \times U(1)$ breaking. Three of the Goldstone bosons are absorbed by the ordinary Higgs mechanism, while the Higgs-like scalar is a pseudo-Goldstone boson. The Higgs mass is generically suppressed by $\mathcal{O}(g/4\pi)$ compared to the scale Λ of the strong dynamics and of the other composite states. This suggests $\Lambda = \mathcal{O}(1 \text{ TeV})$, which is rather low for evading precision electroweak and FCNC constraints. A larger and safer Λ, e.g., 10 TeV, can be achieved by fine-tuning. Alternatively, Λ naturally increases by an order of magnitude (an extra factor of $g/4\pi$) in Little Higgs models, in which the Higgs mass is protected by two symmetries**. Composite Higgs models can often be reinterpreted (i.e., are equivalent to) theories with extra space-time dimensions. In these dual descriptions the massless Higgs fields are identified as gauge fields in the extra dimensions. These ideas, and related issues such as the generation of Yukawa couplings, are reviewed in more detail in (Bhattacharyya, 2011) and in the articles on *Status of Higgs Boson Physics* and on *Dynamical Electroweak Symmetry Breaking* in (Olive et al., 2014). See also Section 8.1.

The various types of new physics mentioned above can affect the Higgs in a number of way. Mixing in extended Higgs sectors can modify the relative strengths of the Yukawa couplings, especially of the up-type quarks relative to the down-type quarks and charged leptons (Section 8.2.5). They can also increase the Higgs width via unobserved decays, allow decays into other exotic modes (Curtin et al., 2014), modify the Higgs self-interactions (Baglio et al., 2013), or lead to Higgs-mediated flavor changing effects (Buras et al., 2010). Heavy particles such as superpartners, additional quarks and leptons, and heavy W' bosons are expected in many extended theories, including most of the composite Higgs models. These can enter into loops and significantly modify gluon fusion and such loop-induced decays as GG, $\gamma\gamma$, and $Z\gamma$, or perturb tree-allowed decays such as $H \to b\bar{b}$. Of course, there may be associated effects such as the direct production of the new heavy particles at

**Operationally, the Little Higgs models involve additional heavy vectors, fermions, and scalars which cancel the one-loop quadratic divergences.

the LHC, modification of the oblique parameters or other aspects of precision electroweak physics, the observation of FCNC, or the modification of high energy VV' scattering, where $V, V' = W$ or Z (e.g., (Baak et al., 2013; Corbett et al., 2014)).

Possible deviations from the SM predictions for the Higgs couplings have been studied quantitatively in specific classes of models and from a model independent or general effective operator framework, e.g., in (Giardino et al., 2014; Ellis and You, 2013; Belanger et al., 2013; Contino et al., 2013; Elias-Miro et al., 2013). Typical deviations are in the 1-10% range. Considerable improvement on the current observations shown in Figures 7.43 and 7.44 are expected from future runs at higher energy at the LHC, especially with a luminosity upgrade. These could reach a precision of $\sim 5 - 10\%$. Even more precise measurements would be possible at a future e^-e^+ collider, such as a proposed International Linear Collider (ILC)[††] (Weiglein et al., 2006). For example, the ILC running at 250 GeV would be able to determine the total H width by measuring the total $e^-e^+ \to ZH$ rate and combining it with the $H \to ZZ^*$ branching ratio. Increasing the ILC energy to 500-1000 GeV would allow measurements of the other couplings, including the $t\bar{t}H$ and HHH couplings, many at the 1% level. Of course, the theoretical predictions of the SM would have to be computed to comparable precision (Denner et al., 2011; Almeida et al., 2014; Lepage et al., 2014; Englert et al., 2014). Future prospects for various facilities are surveyed in (Dawson et al., 2013; Bechtle et al., 2014).

7.6 New References

Aad, G. et al. (2012). Observation of a new particle in the search for the Standard Model Higgs boson with the ATLAS detector at the LHC. *Phys.Lett. B716*, 1–29, arXiv:1207.7214 [hep-ex].

Aad, G. et al. (2013a). Evidence for the spin-0 nature of the Higgs boson using ATLAS data. *Phys.Lett. B726*, 120–144, arXiv:1307.1432 [hep-ex].

Aad, G. et al. (2013b). Measurements of Higgs boson production and couplings in diboson final states with the ATLAS detector at the LHC. *Phys.Lett. B726*, 88–119, arXiv:1307.1427 [hep-ex].

Aad, G. et al. (2014a). Measurement of the Higgs boson mass from the $H \to \gamma\gamma$ and $H \to ZZ^* \to 4\ell$ channels with the ATLAS detector using 25 fb^{-1} of pp collision data. *Phys.Rev. D90*, 052004, arXiv:1406.3827 [hep-ex].

[††] http://www.linearcollider.org/ILC/Publications/Technical-Design-Report.

Aad, G. et al. (2014b). Observation and measurement of Higgs boson decays to WW^* with the ATLAS detector. arXiv:1412.2641 [hep-ex].

Aaltonen, T. et al. (2013). Higgs Boson Studies at the Tevatron. *Phys.Rev. D88*, 052014, arXiv:1303.6346 [hep-ex].

Almeida, L. G., S. J. Lee, S. Pokorski, and J. D. Wells (2014). Study of the 125 GeV Standard Model Higgs Boson Partial Widths and Branching Fractions. *Phys.Rev. D89*, 033006, arXiv:1311.6721 [hep-ph].

Altarelli, G. (2013). The Higgs: so simple yet so unnatural. *Phys.Scripta T158*, 014011, arXiv:1308.0545 [hep-ph].

Baak, M., A. Blondel, A. Bodek, R. Caputo, T. Corbett, et al. (2013). Working Group Report: Precision Study of Electroweak Interactions. arXiv:1310.6708 [hep-ph].

Baglio, J., A. Djouadi, R. Gröber, M. Mühlleitner, J. Quevillon, et al. (2013). The measurement of the Higgs self-coupling at the LHC: theoretical status. *JHEP 1304*, 151, arXiv:1212.5581 [hep-ph].

Baglio, J., O. Eberhardt, U. Nierste, and M. Wiebusch (2014). Benchmarks for Higgs Pair Production and Heavy Higgs Searches in the Two-Higgs-Doublet Model of Type II. *Phys.Rev. D90*, 015008, arXiv:1403.1264 [hep-ph].

Barger, V., P. Langacker, M. McCaskey, M. Ramsey-Musolf, and G. Shaughnessy (2009). Complex Singlet Extension of the Standard Model. *Phys.Rev. D79*, 015018, arXiv:0811.0393 [hep-ph].

Bechtle, P., S. Heinemeyer, O. Stl, T. Stefaniak, and G. Weiglein (2014). Probing the Standard Model with Higgs signal rates from the Tevatron, the LHC and a future ILC. *JHEP 1411*, 039, arXiv:1403.1582 [hep-ph].

Belanger, G., B. Dumont, U. Ellwanger, J. Gunion, and S. Kraml (2013). Global fit to Higgs signal strengths and couplings and implications for extended Higgs sectors. *Phys.Rev. D88*, 075008, arXiv:1306.2941 [hep-ph].

Bernardi, G. and M. Herndon (2014). Searches for the Standard Model Higgs Boson at Hadron Colliders at $\sqrt{s} = 2$, 7 and 8 TeV until the Discovery of the 125 GeV Boson. *Rev.Mod.Phys. 86*, 479, arXiv:1210.0021 [hep-ex].

Bezrukov, F., M. Y. Kalmykov, B. A. Kniehl, and M. Shaposhnikov (2012). Higgs Boson Mass and New Physics. *JHEP 1210*, 140, arXiv:1205.2893 [hep-ph].

Bhattacharyya, G. (2011). A Pedagogical Review of Electroweak Symmetry Breaking Scenarios. *Rept.Prog.Phys. 74*, 026201, arXiv:0910.5095 [hep-ph].

Bolognesi, S., Y. Gao, A. V. Gritsan, K. Melnikov, M. Schulze, et al. (2012). On the spin and parity of a single-produced resonance at the LHC.

Phys.Rev. D86, 095031, arXiv:1208.4018 [hep-ph].

Branco, G., P. Ferreira, L. Lavoura, M. Rebelo, M. Sher, et al. (2012). Theory and phenomenology of two-Higgs-doublet models. *Phys.Rept. 516*, 1–102, arXiv:1106.0034 [hep-ph].

Buchmueller, O., M. Dolan, J. Ellis, T. Hahn, S. Heinemeyer, et al. (2014). Implications of Improved Higgs Mass Calculations for Supersymmetric Models. *Eur.Phys.J. C74*(3), 2809, arXiv:1312.5233 [hep-ph].

Buras, A. J., M. V. Carlucci, S. Gori, and G. Isidori (2010). Higgs-mediated FCNCs: Natural Flavour Conservation vs. Minimal Flavour Violation. *JHEP 1010*, 009, arXiv:1005.5310 [hep-ph].

Buttazzo, D., G. Degrassi, P. P. Giardino, G. F. Giudice, F. Sala, et al. (2013). Investigating the near-criticality of the Higgs boson. *JHEP 1312*, 089, arXiv:1307.3536.

Carena, M., S. Heinemeyer, O. Stl, C. Wagner, and G. Weiglein (2013). MSSM Higgs Boson Searches at the LHC: Benchmark Scenarios after the Discovery of a Higgs-like Particle. *Eur. Phys. J. C73*, 2552, arXiv:1302.7033 [hep-ph].

Chatrchyan, S. et al. (2012). Observation of a new boson at a mass of 125 GeV with the CMS experiment at the LHC. *Phys.Lett. B716*, 30–61, arXiv:1207.7235 [hep-ex].

Chatrchyan, S. et al. (2013). Observation of a new boson with mass near 125 GeV in pp collisions at $\sqrt{s} = 7$ and 8 TeV. *JHEP 1306*, 081, arXiv:1303.4571 [hep-ex].

Chatrchyan, S. et al. (2014). Measurement of the properties of a Higgs boson in the four-lepton final state. *Phys.Rev. D89*, 092007, arXiv:1312.5353 [hep-ex].

Contino, R., M. Ghezzi, C. Grojean, M. Muhlleitner, and M. Spira (2013). Effective Lagrangian for a light Higgs-like scalar. *JHEP 1307*, 035, arXiv:1303.3876 [hep-ph].

Corbett, T., O. Eboli, and M. Gonzalez-Garcia (2014). Unitarity Constraints on Dimension-Six Operators. arXiv:1411.5026 [hep-ph].

Craig, N., J. Galloway, and S. Thomas (2013). Searching for Signs of the Second Higgs Doublet. arXiv:1305.2424 [hep-ph].

Curtin, D., R. Essig, S. Gori, P. Jaiswal, A. Katz, et al. (2014). Exotic decays of the 125 GeV Higgs boson. *Phys.Rev. D90*(7), 075004, arXiv:1312.4992 [hep-ph].

Dawson, S., A. Gritsan, H. Logan, J. Qian, C. Tully, et al. (2013). Higgs Working Group Report of the Snowmass 2013 Community Planning Study.

arXiv:1310.8361 [hep-ex].

Degrassi, G., S. Di Vita, J. Elias-Miro, J. R. Espinosa, G. F. Giudice, et al. (2012). Higgs mass and vacuum stability in the Standard Model at NNLO. *JHEP 1208*, 098, arXiv:1205.6497 [hep-ph].

Denner, A., S. Heinemeyer, I. Puljak, D. Rebuzzi, and M. Spira (2011). Standard Model Higgs-Boson Branching Ratios with Uncertainties. *Eur.Phys.J. C71*, 1753, arXiv:1107.5909 [hep-ph].

Dittmaier, S. and M. Schumacher (2013). The Higgs Boson in the Standard Model - From LEP to LHC: Expectations, Searches, and Discovery of a Candidate. *Prog.Part.Nucl.Phys. 70*, 1–54, arXiv:1211.4828 [hep-ph].

Djouadi, A. (2008a). The Anatomy of electro-weak symmetry breaking. I: The Higgs boson in the standard model. *Phys. Rept. 457*, 1–216, arXiv:hep-ph/0503172.

Djouadi, A. (2008b). The Anatomy of electro-weak symmetry breaking. II. The Higgs bosons in the minimal supersymmetric model. *Phys. Rept. 459*, 1–241, arXiv:hep-ph/0503173.

Djouadi, A., M. Drees, U. Ellwanger, R. Godbole, C. Hugonie, et al. (2008). Benchmark scenarios for the NMSSM. *JHEP 0807*, 002, arXiv:0801.4321 [hep-ph].

Djouadi, A., M. Spira, and P. Zerwas (1991). Production of Higgs bosons in proton colliders: QCD corrections. *Phys.Lett. B264*, 440–446.

Draper, P., P. Meade, M. Reece, and D. Shih (2012). Implications of a 125 GeV Higgs for the MSSM and Low-Scale SUSY Breaking. *Phys.Rev. D85*, 095007, arXiv:1112.3068 [hep-ph].

Eichten, E., K. Lane, and A. Martin (2012). A Higgs Impostor in Low-Scale Technicolor. arXiv:1210.5462 [hep-ph].

Elias-Miro, J., J. Espinosa, E. Masso, and A. Pomarol (2013). Higgs windows to new physics through d=6 operators: constraints and one-loop anomalous dimensions. *JHEP 1311*, 066, arXiv:1308.1879 [hep-ph].

Ellis, J. (2013). Higgs Physics. arXiv:1312.5672 [hep-ph].

Ellis, J. and T. You (2013). Updated Global Analysis of Higgs Couplings. *JHEP 1306*, 103, arXiv:1303.3879 [hep-ph].

Englert, C., A. Freitas, M. Mhlleitner, T. Plehn, M. Rauch, et al. (2014). Precision Measurements of Higgs Couplings: Implications for New Physics Scales. *J.Phys. G41*, 113001, arXiv:1403.7191 [hep-ph].

Frank, M., L. Selbuz, L. Solmaz, and I. Turan (2013). Higgs bosons in supersymmetric $U(1)'$ models with CP violation. *Phys.Rev. D87*(7), 075007,

arXiv:1302.3427 [hep-ph].

Giardino, P. P., K. Kannike, I. Masina, M. Raidal, and A. Strumia (2014). The universal Higgs fit. *JHEP 1405*, 046, arXiv:1303.3570 [hep-ph].

Hahn, T., S. Heinemeyer, W. Hollik, H. Rzehak, and G. Weiglein (2014). High-precision predictions for the light CP-even Higgs Boson Mass of the MSSM. *Phys.Rev.Lett. 112*, 141801, arXiv:1312.4937 [hep-ph].

Hall, L. J., D. Pinner, and J. T. Ruderman (2012). A Natural SUSY Higgs Near 126 GeV. *JHEP 1204*, 131, arXiv:1112.2703 [hep-ph].

Heinemeyer, S. et al. (2013). Handbook of LHC Higgs Cross Sections: 3. Higgs Properties. arXiv:1307.1347 [hep-ph].

Herrero, M. (2014). The Higgs System in and Beyond the Standard Model. arXiv:1401.7270 [hep-ph].

Khachatryan, V. et al. (2014a). Constraints on the Higgs boson width from off-shell production and decay to Z-boson pairs. *Phys.Lett. B736*, 64, arXiv:1405.3455 [hep-ex].

Khachatryan, V. et al. (2014b). Constraints on the spin-parity and anomalous HVV couplings of the Higgs boson in proton collisions at 7 and 8 TeV. arXiv:1411.3441 [hep-ex].

Khachatryan, V. et al. (2014c). Observation of the diphoton decay of the Higgs boson and measurement of its properties. *Eur.Phys.J. C74* (10), 3076, arXiv:1407.0558 [hep-ex].

Landau, L. (1948). On the angular momentum of a two-photon system. *Dokl.Akad.Nauk Ser.Fiz. 60*, 207–209.

Lepage, G. P., P. B. Mackenzie, and M. E. Peskin (2014). Expected Precision of Higgs Boson Partial Widths within the Standard Model. arXiv:1404.0319 [hep-ph].

Logan, H. E. (2014). TASI 2013 lectures on Higgs physics within and beyond the Standard Model. arXiv:1406.1786 [hep-ph].

Olive, K. A. et al. (2014). Review of Particle Physics (RPP). *Chin.Phys. C38*, 090001, http://pdg.lbl.gov.

Patt, B. and F. Wilczek (2006). Higgs-field portal into hidden sectors. arXiv:hep-ph/0605188 [hep-ph].

Salvio, A. (2013). Higgs Inflation at NNLO after the Boson Discovery. *Phys.Lett. B727*, 234–239, arXiv:1308.2244 [hep-ph].

Schabinger, R. and J. D. Wells (2005). A Minimal spontaneously broken hidden sector and its impact on Higgs boson physics at the large hadron collider. *Phys.Rev. D72*, 093007, arXiv:hep-ph/0509209 [hep-ph].

Yang, C.-N. (1950). Selection Rules for the Dematerialization of a Particle Into Two Photons. *Phys.Rev. 77*, 242–245.

CRC PRESS
Boca Raton Ann Arbor London Tokyo

Index

CRC PRESS
Boca Raton Ann Arbor London Tokyo